Epithelial to Mesenchymal Transition in the Endometrium Mediated by HOXA10 drives Embryo Implantation

Nancy Ashary[1], Sanjana Suresh[1], Anshul Bhide[1], Sharmishtha Shyamal[1,] Pranya N[1], Anuradha Mishra[2], Anuradha A[2], Shruti Hansda[2], Harshavardhan B V[4], Mohit Kumar Jolly[3] and Deepak Modi[1]*

[1]Molecular and Cellular Biology Laboratory, ICMR-National Institute for Research in Reproductive and Child Health, Indian Council of Medical Research (ICMR), JM Street, Parel, Mumbai 400012, India

[2]Department of Zoology, Banaras Hindu University (BHU) in Varanasi, Uttar Pradesh, India, is Varanasi-221005

[3]Department of Bioengineering, Indian Institute of Science (IISc) CV Raman Rd, Bengaluru, Karnataka 560012

[4]IISc Mathematics Initiative, Indian Institute of Science (IISc) CV Raman Rd, Bengaluru, Karnataka 560012

*Corresponding author: deepaknmodi@yahoo.com, modid@nirrh.res.in

Competing Interest Statement: Authors declare no conflict of interest

Abstract

Embryo implantation requires the breaching of the endometrial luminal epithelium (LE) to facilitate invasion. In this study, we report that during implantation, endometrial LE cells undergo partial epithelial-to-mesenchymal transition (pEMT) specifically at the implantation sites. This pEMT in the LE is critical, as the *in vivo* knockdown of the EMT transcription factor *Twist*2 inhibits embryo implantation. Furthermore, we observed a reduction in the expression of the transcription factor HOXA10 in LE cells at the implantation sites. Interestingly, LE cells of HOXA10-hypomorphic mice and human endometrial epithelial cells (RL95-2) with *HOXA10* knockdown (*HOXA10*KD) also undergo pEMT and acquire a migratory phenotype *in vitro*, suggesting that the loss of HOXA10 drives pEMT in the endometrial epithelium. The *HOXA10*KD cells have a higher pEMT score and differential expression of genes associated with cell migration and TGF-β signaling pathways. We also determined the genome-wide occupancy sites of HOXA10 in human endometrial epithelial cells and identified 1,246 direct targets that had significant roles in EMT. Collectively, our findings suggest that HOXA10 is required to maintain an epithelial state and its loss activates mesenchymal genes resulting in a pEMT phenotype. This adds HOXA10 as a member of the MET inducer team that engage in mutually inhibitory feedback loops directly or indirectly with EMT inducer team. In summary, our study establishes that pEMT in the LE as a critical step for embryo implantation and reveals that HOXA10 regulates this process.

Keywords: pEMT, Hybrid EMT, Invasion, Homeobox genes, CUT&RUN, Epithelial-Mesenchymal Plasticity

Introduction

In the evolution of viviparity, the Mullerian derivatives in mammals underwent a series of modifications in order to facilitate the implantation of the blastocyst and its invasion into the uterus, creating a stable feto-maternal interface. To achieve this, uterus must become receptive for the blastocyst to adhere on the endometrial luminal epithelial (LE) cells (1–4). In the receptive stage, the endometrial LE cells are columnar and tightly adhered to each other and form a barrier for invasion. In species with invasive placentation, the embryo embeds in the endometrial stromal bed by breaking this LE barrier (5). The embryo achieves this by extending the projection of the trophoblast cells that penetrate between the LE cells at their intercellular junctions and subsequently adhere to its lateral surfaces. This is followed by breaking the basal lamina and displacement of the LE cells thereby opening the way for the embryo to embed in the stroma (6). It was believed that the LE cells proximal to the blastocyst undergo apoptosis and these dead cells are phagocytosed by the trophoblast cells paving the way for the embryo into stromal bed (7–9). However, apoptotic cells and Caspase3 activation are not commonly seen in the LE cells juxtaposed to the embryo indicating that apoptosis is not a major mechanism of LE clearance (10). Instead, it is proposed that the LE cells either die by necroptosis and then phagocytosed by the trophoblasts or live LE cells undergo entosis by the trophoblast cells to initiate invasion (10, 11). Irrespective of whether live or dead cells are engulfed by the trophoblasts, major morphological changes in the LE cells are observed at the time of embryo implantation. As compared to the receptive endometrium where the LE cells exhibit polarity, upon embryo apposition, there is a reduction in lateral adhesions and desmosome numbers between the LE cells, there is redistribution of adherent junction molecules like cadherins, and there is cytoskeletal remodeling suggestive of a loss of apico-basal cell polarity of the LE (2, 12–18). Interestingly these changes are conserved in most species irrespective of the type of implantation indicating that loss of apico-basal polarity of LE cells is an evolutionarily conserved phenomenon during embryo implantation (19). Indeed, mice knockout for *Vangl2* (a gene essential for planar cell polarity) are sub fertile due to altered polarity of the LE cells (20, 21). In many tissues, loss of epithelial cell polarity is associated with epithelial-to-mesenchymal transition (EMT) (22, 23). Along with loss of polarity, cells undergoing EMT have reduced cell-cell adhesion and reduced levels of epithelial markers (like E-cadherin), gain of mesenchymal markers (like N-cadherin and EMT-related transcription factors), and the cells acquire a migratory property (24). While EMT was assumed to be a binary process where the cells may be either in epithelial or mesenchymal states, recent studies have also shown that in many instances the cells acquire a partial or hybrid EMT phenotype

(also referred to as EMT plasticity or EMP). The hybrid or partial EMT (pEMT) cells co-express both epithelial and mesenchymal markers in varying degrees and a distinct combination of EMT transcription factors (EMT-TFs) that are essential to acquire the stable pEMT phenotype (25–27).

In the context of embryo implantation, some evidence suggests the occurrence of EMT in the LE. Reduction in E-cadherin expression in the LE at the time of blastocyst attachment is observed in most species irrespective of the type of implantation (19, 28). In *in vitro* implantation assays, a reduction in epithelial markers like integrins and E-cadherin and upregulation of the mesenchymal markers like N-cadherin and vimentin are observed in the endometrial epithelial cells in response to trophoblast spheroids implying that EMT occurs in the LE at the time of embryo implantation (29–31). However, whether these LE cells undergo complete transition to a mesenchymal phenotype or acquire a hybrid state is not known. The molecular mechanisms that drive EMT in the endometrial epithelium for embryo implantation are unknown.

Herein, we report that pEMT occurs in the LE at the site of implantation and blocking this process leads to the failure of the embryo to breach the LE. We further show that pEMT requires the loss of the transcription factor HOXA10 to drive the mesenchymal program while partly retaining the epithelial program.

Materials and Methods:

Ethics Statement and Animal Tissue Collection

The use of animals was approved by the Institutional Animal Ethical Committee of ICMR-NIRRCH (project numbers 18/17 and 04/22) and Banaras Hindu University (BHU/DoZ/IAEC/2018-19/035). Adult (6–8-weeks old) C57BL/6 female mice housed in the experimental animal facility of ICMR-NIRRCH were mated with males of proven fertility and the day of vaginal plug was designated as day 1 of pregnancy. Uteri were collected on Day 4 (D4 09:00h), Day 5 morning (D5 09:00h), Day 5 evening (D5 21:00h) and Day 5 midnight (D5 24:00h). These time points were chosen as they span the period of receptivity, apposition, and implantation in mice (10). HOXA10 hypomorphs are mice transgenic for a *Hoxa10* shRNA and have reduced expression of HOXA10 in their uteri as compared to their wild-type counterparts (SI Appendix, Materials and Methods S1 and Fig. S1). The development and characterization of these mice are detailed elsewhere (32). These animals were housed at the Experimental Animal Facility of ICMR-NIRRCH and the uteri were collected from either non-pregnant or on D5 (09:00h) of transgenic animals. The uteri from non-transgenic littermates

were used as wild-type controls. Adult female golden hamsters (*Mesocricetus auratus)* housed in the animal house facility of BHU were mated with fertile males and the day of detection of sperm in a vaginal smear was considered as day 1 of pregnancy. Uteri from these animals were collected on day 5 (D5) which coincides with the day of implantation in this species (33).

Histology and Immunofluorescence

Uteri at designated time points were collected and fixed in 4% paraformaldehyde (PFA, Sigma-Aldrich), paraffin-embedded and sectioned. The sections were stained using Hematoxylin and Eosin as detailed earlier (34). Multiplex immunofluorescence was performed on paraffin sections using a commercial kit (PerkinElmer or Biotium), as described previously (35). The details of the antibodies used in the study and their optimized dilutions are given in (SI Appendix, Table. S1). Briefly, uterine sections were deparaffinized, and blocked in 2% Bovine Serum Albumin (BSA, Sigma-Aldrich). The antigenic sites were unmasked by incubating the sections in Tris-EDTA buffer (10 mM, pH 9) at 90°C for 30 min and probed with primary antibody. Post-washing, the sections were incubated with HRP conjugated secondary antibody, followed by tyramide signal amplification (TSA)-conjugated fluorophores for signal detection. For multiplexing, after the first round of probing, the sections were incubated for 30 min at 90 °C in the Tris-EDTA buffer and probed with the next antibody. The sections were counterstained with DAPI (Sigma-Aldrich) and mounted with EverBrite™ Hardset Mounting Medium (Biotium). For immunofluorescence on cultured cells, they were trypsinized and seeded on sterilized coverslips and cultured till the desired confluency. Cells were fixed in chilled 70% methanol, washed, blocked in BSA and then incubated with primary antibody overnight at 4°C. Next day, after washing, the cells were incubated with fluorescently conjugated secondary antibody (Invitrogen), and the nuclei were counterstained with DAPI and mounted as above.

Imaging was done on an inverted fluorescence microscope equipped with sCMOS camera (Leica Microsystems DMi8, Germany). The images were analyzed, and fluorescence intensities from selected areas were quantified in Leica Microsystems using LAS X software. Five independent areas of LE in non-consecutive sections were selected using the Region of Interest (ROI) function and the intensities of the desired signals were estimated. For estimating co-expression, the multi-colored images were imported in ImageJ (Fiji) and JACoP Co-localization plugin was used to determine the Pearson's correlation coefficient in the LE cells. For single-cell quantification, each LE cell surrounding the embryo was individually selected using the ROI function, and the fluorescence intensities were estimated using LAS X software. At least 50 non-overlapping cells per implantation site were quantified.

Knockdown of *Twist2 in vivo*

200ng of *Twist2* esiRNA or scrambled esiRNA (both from Sigma-Aldrich) was incubated in Lipofectamine 3000 (Invitrogen) reagent and 20 µl of the complex was delivered intraluminally into the uterus of day 3 (D3) pregnant mice using the NSET™ device (ParaTechs) as per the manufacturer's instructions. Briefly, the NSET device was attached to a pipette and the large speculum was used to hold open the vagina and visualize the cervix. The NSET tip was inserted up to the utero-cervical junction and the solution was expelled. After 48 or 72h of administration (D5 or D6 of pregnancy) the uteri were collected, fixed, and processed as above for serial sectioning. The numbers of implantations per animal were estimated in uterine sections by counting the number of implantation crypts (on D5) or embryos embedded in the uterine stroma (on D6). For each animal, every 5th slide was assessed and at least 10 slides/animal were evaluated. The sequence of *Twist2* esiRNA is given in (SI Appendix, Table. S2). The efficiency of knockdown in the uterine sections was determined using immunofluorescence for TWIST2.

HOXA10 Knockdown in the Endometrial Epithelial Cells

RL95-2 cell line (henceforth referred to as RL95) are human endometrial epithelial cells and highly adhesive to trophoblast spheroids and are considered a suitable model to investigate human embryo implantation *in vitro* (36–38). RL95 cells (ATCC-CRL-1671) were cultured on gelatin-coated plates in DMEM-F12 (Gibco) and 10% fetal bovine serum (FBS, Gibco). To silence HOXA10, cells were transfected with a plasmid containing a *HOXA10* shRNA (V3LHS_300885; Dharmacon) or a scrambled shRNA (V3LHS_65890S; Dharmacon) using X-tremeGENE™ HP DNA Transfection Reagent (Roche). Both these plasmids have been prevalidated *in vitro* and *in vivo* (32). After 48h of transfection, the cells were challenged with 2ug/ml of puromycin (Gibco) for 48h, and the surviving cells were sub-cultured and used for further experiments. The knockdown efficiency of HOXA10 was examined by qPCR (S1 Appendix, Material and Methods S2 and Fig.S2). Cells were regularly tested for mycoplasma using PCR (HiMedia).

Time-Lapse Microscopy for Cell Migration

Cells knockdown for HOXA10 (*HOXA10*KD) and scrambled (control) were seeded into 96-well microplates (Revvity) and cultured in DMEM-F12 medium containing 10% FBS and 2ug/ml puromycin. The next day, cells were imaged every 30 min for 24 h using the Operetta CLS High-Content Analysis system equipped with 37 °C, 5% CO2 environmentally controlled chamber (Revvity). Chemotaxis and migration plugins (Harmony High-Content Imaging and Analysis Software) were used to estimate cell migration and displacement.

Spheroid Induced Cell Displacement Assay

To test if embryonic spheroids have an effect on the displacement and migration of endometrial epithelial cells, spheroid induced cell displacement assay was performed as described in (39), with minor modifications. Briefly, mycoplasma free trophoblast cells (HTR8/SV-neo cells ATCC-CRL-3271) cultured in DMEM-F12 and 10% FBS were seeded in low attachment plates (PerkimElmer) and 24h later the spheroids were labeled with CellTracker™ Red CMTPX (Invitrogen). Approximately 5 spheroids per well were co-cultured with monolayers of CellTracker™ Green CMFDA (Invitrogen) labeled control or *HOXA10*KD cells. After 24h the wells were imaged under a fluorescence microscope (Leica Microsystems DMi8).

For live cell imaging, the *HOXA10*KD cells were seeded into 96-well microplates (PerkinElmer) and grown until 90% confluency. Trophoblast spheroids were allowed to attach to these cells for 2h and the endometrial cells in the area of the spheroids were imaged every 30 min for 12h in the Operetta CLS High-Content screening system. The cell migration patterns were analyzed using Harmony High-Content Imaging and Analysis Software.

RNAseq

RNA was isolated from 70% confluent *HOXA10*KD and control endometrial epithelial cells using the RNEasy mini kit. High-quality RNA (RIN values >9) was subjected to standard paired-end RNA-Seq library preparation using NEBNext® Ultra™ II Directional RNA Library Prep Kit (NEB-E7760S). Sequencing was performed on an Illumina NovaSeq 6000 platform at Bionivid Technology (Bangalore, India). Low-quality reads were trimmed and the raw sequence data was processed, and aligned to the human reference genome (hg38). Raw counts were calculated using Feature Counts and differential gene expression (DEGs) analysis was performed using EdgeR. Genes with a Log2 fold change ± 2 and a P-adjusted value of 0.05 were considered as differentially expressed.

Identification of HOXA10 Occupancy in Endometrial Epithelial Cells using CUT&RUN

Mycoplasma free endometrial epithelial cells (RL95 cells) were treated with estrogen (10^{-8}M) and progesterone (10^{-6}M) (both Sigma-Aldrich) for 48h. Preliminary experiments had shown that at these concentration HOXA10 expression is robustly increased in RL95 cells. The cells were collected by trypsinization and subjected to CUT&RUN using a commercial kit (CUT&RUN Assay Kit #86652 Cell Signaling Technology). Briefly, 100,000 cells were lysed and nuclei were washed thrice and incubated overnight at 4°C with a validated HOXA10 antibody (50ug). The validation of this antibody is provided in (SI Appendix, Fig. S3). Excess primary antibody was removed by multiple washings and the nuclei were incubated with a pAG-MNase. It was activated with $CaCl_2$ at 4°C to initiate DNA digestion for 30 min and then

stopped using the stop buffer. The released DNA fragments were purified using the conventional phenol-chloroform DNA extraction method. DNA library preparation was done as detailed (40) and sequencing on NovaSeq 6000 platform was outsourced (Clevergene, Bangalore, India). High-quality reads were aligned to the human reference genome (hg38), and peak calling was performed using SEACR, with the green list employed as a control (41). The top 10,000 peaks were annotated, and motif enrichment analysis was conducted using the MEME suite.

RNAseq and CUT&RUN Data Analysis and Visualization

Gene enrichment analysis of DEGs was performed using WebGestalt (42), and pathways of interest were visualized using KEGG Mapper (43). Data visualization included Integrative Genomics Viewer (IGV), heatmaps, volcano plots, Sankey plots, alluvial plots, and bubble plots. These visualizations were generated using the ggplot2 and SRPlot packages within the R statistical environment. Protein-protein interaction (PPI) networks were constructed using the Cytoscape StringApp. The single-sample gene set enrichment analysis (ssGSEA) algorithm (44), as implemented in GSEAPy (45), was used to calculate ssGSEA scores for the partial EMT (pEMT) signature (46). Pearson correlations between gene expression levels and either HOXA10 expression or pEMT scores were computed using the Pearson function from the SciPy library (47).

Statistics

The mean ± SD for all the experimental data was calculated and statistical analysis was done by Student's t-test and one way ANOVA using GraphPad Prism, version 8. $p<0.05$ was accepted as statistically significant.

Results

Embryo Implantation is Associated with EMT in the Endometrial Luminal Epithelium

Histologically, in the receptive phase (D4 09:00h) when the embryo is floating in the uterine lumen, the LE cells were columnar (Fig. 1 A). When the embryo was apposed (D5 09:00h), the LE cells were same as D4. However, on D5 21:00h, the LE cells were flattened and their height significantly reduced (Fig. 1 A and B). This reduction in cell height was associated with an increase in inter-nuclear distance (Fig. 1 B, n=5 animals/time point). This effect was specific to the implantation sites as the cells of the LE at the inter-implantation site (on D5 21:00h) were columnar and similar to those seen at the receptive phase (D4 09:00h) (SI Appendix, Fig.S4).

Since epithelial cell flattening is a sign of EMT we stained the sections for epithelial (E-Cad and KRT8) and mesenchymal markers (N-Cad and ZEB2) and observed that on D4 (09:00h) the LE cells were positive for E-Cad and KRT8 and negative for N-Cad and ZEB2 (Fig. 1 C and D, n=5). However, on D5 (09:00h), the LE cells at the implantation sites were positive for the mesenchymal markers (N-Cad and ZEB2), and the expression of epithelial markers (E-Cad and KRT8) was lower than that observed on D4 (09:00h) (Fig. 1 C and D, n=5). Quantitatively, as compared to D4, there was almost a 50% reduction in the intensity of E-Cad and KRT8 in the LE cells on D5 and this reduction was statistically significant (Fig. 1 E, n=5 animals/time point, $p<0.0001$).

The suppression of epithelial markers and activation of mesenchymal markers was specific to the implantation sites as the mesenchymal markers (N-Cad and ZEB2), were not detected in the LE cell at the inter-implantation sites (Fig. 1 D) and the levels of E-Cad and KRT8 were higher at the inter-implantation sites as compared to implantation sites (n=5 animals/time point, $p <0.0001$) and were comparable to those on D4 (Fig. 1 E).

To determine if the expression of mesenchymal markers in the LE at the time of implantation also occurs in other species with invasive implantation, we tested their expression in non-pregnant (NP) and implantation stage (D5) hamster endometrium. The results revealed that the expression of E-Cad was diffused in the LE of D5 hamsters at implantation site as compared to non-pregnant uteri (Fig. 1 F), N-Cad was detected only in the LE of hamsters on D5 at implantation site (Fig. 1 F). E-Cad in the LE cell at the inter-implantation sites were similar to non-pregnant uteri with no N-Cad expression (Fig. 1 F, n=3 animals/time point). Together these results imply that EMT occurs specifically in the LE cells at the site of embryo implantation.

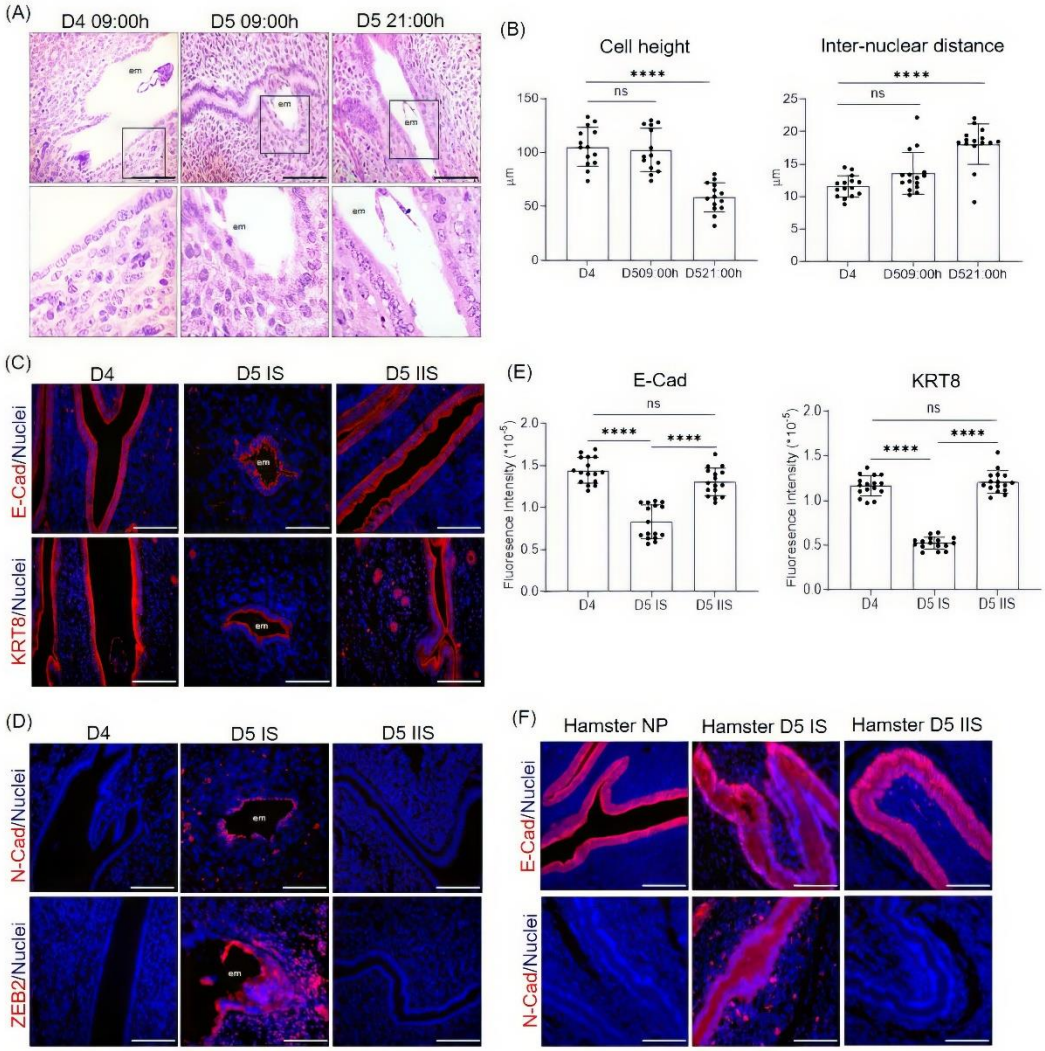

Fig. 1. Endometrial luminal epithelium undergoes Epithelial to Mesenchymal Transition (EMT) at the time of embryo implantation

(A) Hematoxylin and Eosin stained sections of the mouse uterus at the implantation site (IS) on D4 09:00h, D5 09:00h and D5 21:00h. The selected area is boxed and zoomed. (B) Quantification of cell height (µm) and inter-nuclear distance (µm) at IS on D4 (09:00h), D5 (09:00h) and D5 (21:00h). Each dot represents the value of a single region of interest and data of 3 independent regions from multiple sections of 5 animals are plotted. (C) Immunofluorescence for epithelial markers E-Cad and KRT8 on D4 (09:00h) and D5 (09:00h) at the IS and inter-implantation sites (IIS). (D) Immunofluorescence for mesenchymal markers N-Cad and ZEB2 on D4 (09:00h) and D5 (09:00h) at the IS and IIS. (E) Quantification of immunostaining for E-Cad and KRT8. Each dot represents fluorescence intensity in a single region of interest and data of 3 independent regions from multiple sections of 5 animals are plotted. (F) Immunofluorescence for E-Cad and N-Cad in hamster uterus of NP (non-pregnant),

D5 IS and D5 IIS. em = embryo, Scale bar = 100µm. **** is $p<0.0001$, ns= non-significant, mean ±SD values are shown.

Partial EMT (pEMT) in the Luminal Epithelium at the Time of Embryo Implantation

In many instances the cells undergo EMT and do not acquire a complete mesenchymal profile but rather stably adopt a mix of epithelial (e.g. cell-cell adhesion) and mesenchymal (e.g. migration) traits and they also co-express markers of both these states and defined as hybrid EMT or pEMT (48). To determine if the cells of LE at the implantation sites are in a pEMT state, we performed double immunofluorescence for E-Cad and N-Cad. The results revealed that on D4 09:00h, the LE cells were positive for only E-Cad and was localized on the lateral boundaries (Fig. 2 A). However, on D5 09:00h at the site where the embryo apposed, E-Cad expression became diffused and many LE cells were positive for N-Cad. By D5 21:00h E-Cad was again detected laterally in the LE cells; almost all the cells were also positive for N-Cad (Fig. 2 A, Pearson correlation= 0.789, n=5 animals). On D5 24:00h, LE cells at the implantation site also tested positive for both markers. (Fig. 2 A). Bulk quantification of the E-Cad and N-Cad signals in the LE at the implantation sites revealed that as compared to D4, the expression of E-Cad reduced on the morning of D5, which declined further by the evening on the same day, the expression of N-Cad progressively increased during this period. By midnight, (D5 24:00h) the expression of both E-Cad and N-Cad intensified in all the LE cells at the implantation sites (Fig. 2 B). Single cell quantification of the LE cells in the implantation site on D5 21:00h demonstrated that the cells juxtaposed to the embryo strongly co-expressed both E-Cad and N-Cad, and the cells away from the embryo had varying levels of both these markers (Fig. 2 C). In the hamster uterus, at the implantation sites, E-Cad was diffused in most LE cells and they also co-expressed N-Cad, (Fig. 2 D, Pearson correlation=0.5, n=3). In the inter-implantation sites, the cells were strongly E-Cad positive and were negative for N-Cad (Fig. 2 D). Together these results imply that embryo implantation is associated with pEMT in the LE specifically at the implantation sites.

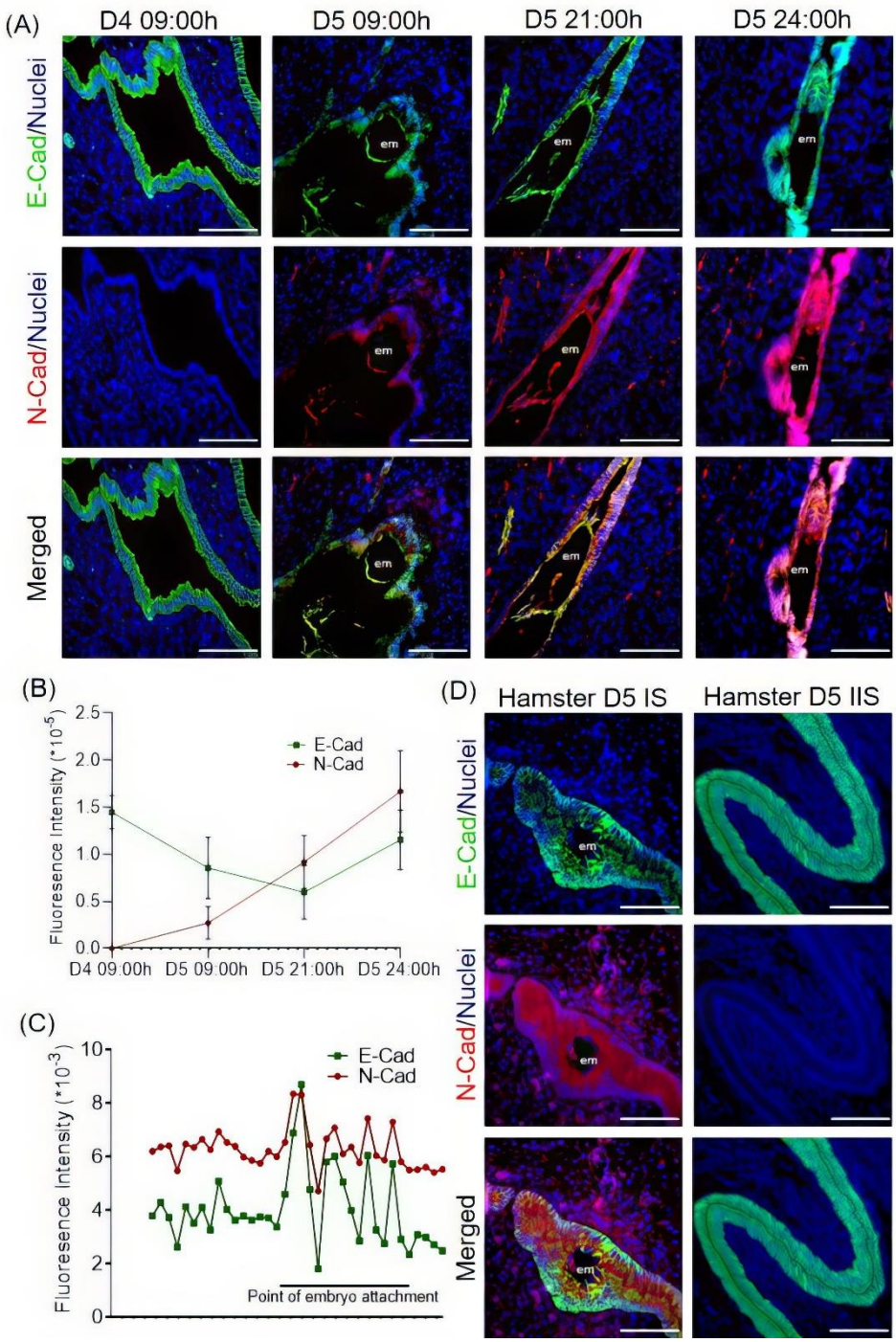

Fig. 2: Embryo implantation involves partial EMT (pEMT) in the endometrial luminal epithelium

(A) Co-immunostaining for E-Cad and N-Cad in mouse uterus on D4 09:00h, D5 09:00h, D5 21:00h and D5 24:00h. (B) Quantification of immunostaining for E-Cad and N-Cad. values are mean ±SD and n=5 animals per group. (C) Spatial distribution of endometrial epithelial cells in different pEMT states at the site of embryo attachment on D5 21:00h. (D) Co-immunostaining for E-Cad and N-Cad in the hamster uterus on D5 at the implantation site (IS) and inter-implantation site (IIS). em = embryo, Scale bar = 100µm.

TWIST2 is Essential for Embryo Implantation

A core set of transcription factors in various combinations orchestrate the EMT program. The core members of EMT-TFs include the members of the SNAI, ZEB and TWIST family which activates the mesenchymal program and/or suppress the epithelial genes to drive EMT. We profiled the expression of SNAIL, SLUG, ZEB1, ZEB2 and TWIST2 in the D4 and D5 uterus. None of the EMT-related transcription factors were detected in the LE of the D4 uterus. However, on the morning of D5 there was an initiation in the expression of TWIST2, SNAIL (Fig. 3 A) and ZEB2 (Fig. 1 D), but not SLUG and ZEB1 in the LE at the implantation sites (Fig. 3 A). We knocked down *Twist2* expression *in vivo* in the endometrium to assess if EMT is essential for implantation. In the scrambled esiRNA treated controls (n=3), on D5, TWIST2 was abundantly expressed, but its expression was significantly ($p<0.0001$) reduced in the LE of mice treated with *Twist2* esiRNA (Fig. 3 B and C, n=3). As compared to scrambled controls, the numbers of implantation site were fewer in the *Twist2*KD uteri (Fig. 3 D, n=5, $p<0.001$). Histologically, On D5, in the scrambled controls, the embryos were in the implantation crypt, however in the *Twist2* esiRNA treated group, the shape of the implantation crypt was abnormal (Fig. 3 E). On D6, in the scrambled esiRNA controls, the LE was cleared and embryos were embedded in the endometrial bed (Fig. 3 E), however in the *Twist2* esiRNA treated group the LE was intact, similar to that seen in D5 uteri (Fig. 3 E). These results imply that at the implantation sites, the LE cells undergo pEMT by activation of TWIST2 and this is essential for epithelial breaching for embryo implantation.

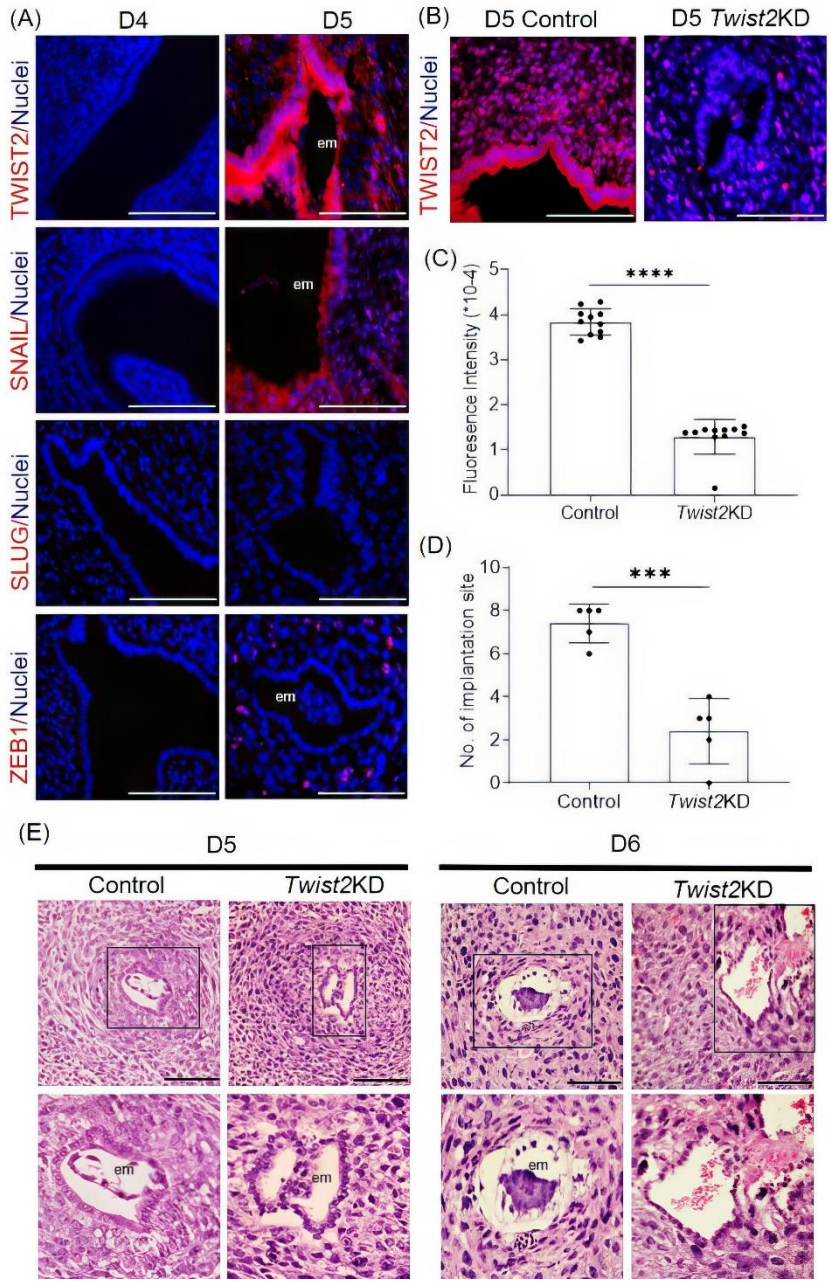

Fig. 3: TWIST2 is essential for embryo implantation

(A) Immunofluorescence for EMT transcription factors TWIST2, SNAIL, SLUG, and ZEB1 on D4 (09:00h) and D5 (09:00h) in the mouse uterus. (B) Immunofluorescence (on D5 09:00h) for TWIST2 in the uteri of mice treated with scramble esiRNA (control) and Twist2 esiRNA (*Twist2*KD). (C) Quantification of immunostaining for TWIST2 in control and *Twist2*KD (n=3). (D) Quantification of the number of implantation sites in control and *Twist2*KD (n=5). (E) Hematoxylin and Eosin-stained sections of control and *Twist2*KD mouse uterus on D5 and D6. Boxed images are zoomed below. em = embryo, Scale bar = 100µm. **** is $p<0.0001$ and *** is $p<0.001$ with mean ±SD values are shown.

Downregulation of HOXA10 Drives pEMT in the Endometrial Epithelium

HOXA10 is a transcription factor essential for embryo implantation and decidualization in the endometrium (2, 49, 50). However, the expression of HOXA10 is downregulated in the LE of the monkey endometrium at the time of implantation (51, 52). In endometrial epithelial cells, HOXA10 binds to E-Cad promoter to upregulate its expression (53), and in endometrial cancer cells, overexpression of HOXA10 drives mesenchymal to epithelial transition (MET) (54). These observations prompted us to investigate if EMT induced in the LE at the time of implantation is due to loss of HOXA10. In line with our earlier observations (52), herein we observed that as compared to D4, HOXA10 levels in the LE cells was reduced in the morning of D5 which is reduced further by 80% in the evening of D5 (Fig. 4 A and B, n=3 animals/time point, $p < 0.0001$). No such reduction was noted at the inter-implantation sites in mouse uterus (SI Appendix, Fig. S5). In the hamster uteri, as compared to non-pregnant controls, the expression of HOXA10 was downregulated in the LE on D5 at the implantation sites, this reduction was almost 50% and was statistically significant (Fig. 4 C and D) and no such reduction was seen on D5 inter-implantation site (Fig. 4 C and D, n=3 animals per time point, $p<0.0001$).

To determine if the reduction in HOXA10 leads to pEMT in the endometrium, the expression of E-Cad and N-Cad was investigated in the uteri of HOXA10 hypomorphs (Fig. 4 E). These mice were generated by overexpressing an shRNA against *Hoxa10* and the uteri of these animals have lower HOXA10 levels as compared to their wildtype counterparts. In the wildtype (n=5), E-Cad expression was detected in the LE cells, there was no N-Cad expression. In all the hypomorphs tested (n=5), there was co-expression of E-Cad and N-Cad in almost all the LE cells of the endometrium (Fig. 4 E, Pearson correlation= 0.7). These results imply that the downregulation of HOXA10 drives pEMT in the endometrial epithelium.

To determine if the downregulation of HOXA10 in endometrial epithelial cells (RL95) is sufficient to drive EMT, we knocked down its expression in the human endometrial epithelial cell line. As compared to the scrambled shRNA (control), in the cells expressing *HOXA10* shRNA (*HOXA10*KD), there was a 70% reduction in *HOXA10* mRNA ($p < 0.005$, n=3, SI Appendix, Fig. S2). The control cells (n=3), abundantly expressed E-Cad and did not express N-Cad (Fig. 4 F). In the *HOXA10*KD (n=3), E-Cad expression was reduced and all the cells co-expressed both E-Cad and N-Cad (Fig. 4 F). Quantitatively the levels of E-Cad were downregulated in *HOXA10*KD cells as compared to controls (n=3, $p<0.001$) and N-Cad was upregulated in HOXA*10*KD cells as compared to control (Fig. 4 G, n=3, $p<0.0001$). Together,

these results indicated that HOXA10 is downregulated at the time of embryo implantation and this loss is essential to drive pEMT.

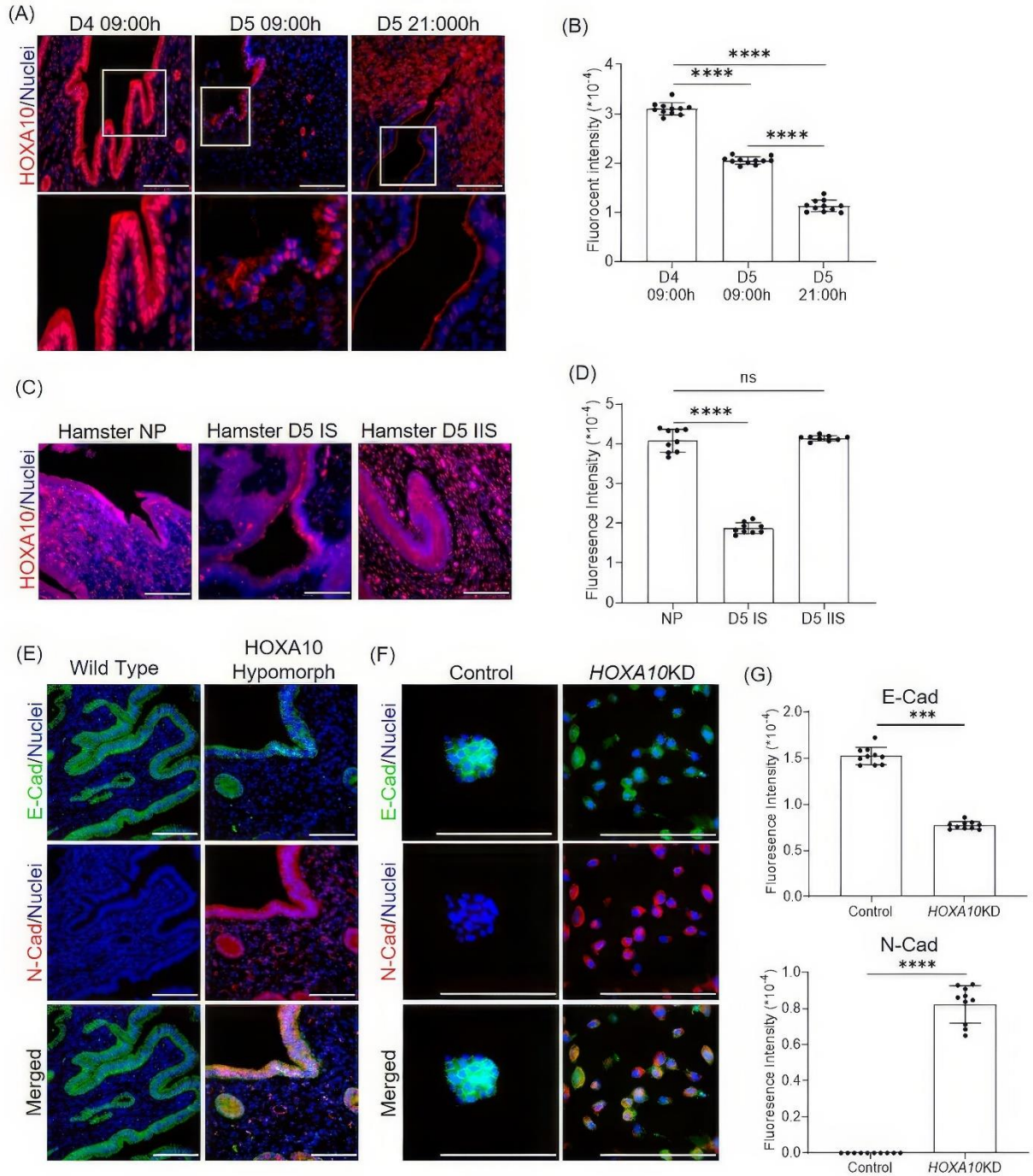

Fig. 4: Loss of HOXA10 drives partial EMT (pEMT) in the luminal epithelial cells

(A) Immunofluorescence for HOXA10 in mouse uterus on D4 09:00h, D5 09:00h and D5 21:00h. Selected area is boxed and zoomed. (B) Quantification of immunostaining for HOXA10 in the mouse uterus. Each dot represents fluorescence intensity in a single region of interest and data of 3 independent regions from multiple sections of 3 animals are plotted. (C) Immunofluorescence for HOXA10 in hamster uterus of NP (non-pregnant), D5 Implantation

site (IS) and inter-implantation site (IIS). (D) Quantification of HOXA10 signals in the hamster uterus. Each dot represents fluorescence intensity in a single region of interest and data of 3 independent regions from multiple sections of 3 animals are plotted. (E) Co-immunostaining for E-Cad and N-Cad in wildtype and HOXA10 hypomorph mouse uterus at diestrus stage. (F) Co-immunostaining for E-Cad and N-Cad in control and *HOXA10*KD endometrial epithelial cells (RL95). (G) Quantification for E-Cad and N-Cad in control and *HOXA10*KD endometrial epithelial cells. Each dot represents fluorescence intensity in a single region of interest and data of 3 independent replicates are plotted. em = embryo, Scale bar = 100µm. **** is $p<0.0001$ and *** is $p<0.001$ with mean ±SD values are shown.

Reduction in HOXA10 Promotes Migration of Endometrial Epithelial Cells

Since cells undergoing EMT acquire a migratory potential, we sought to determine if loss of HOXA10 leads to migration of the human endometrial epithelial cells (RL95). The results revealed that the control cells were non-motile and did not show displacement, most *HOXA10KD* cells were migratory and showed large displacement in all directions (Fig. 5 A, Movie S1 and S2).

To determine if the loss of HOXA10 promotes epithelial cell displacement in response to the embryo, HTR8/SV-neo cell spheroids were cultured on confluent monolayers of control and *HOXA10*KD human endometrial epithelial cells (Fig. 5 B). At the end of 24h of co-culture, the control cells were not displaced by the trophoblast spheroids, however, a large area of clearance was noted in case of *HOXA1*0KD (Fig. 5 B, n=3). To understand the displacement kinetics further, we performed real-time imaging of the co-cultures of the trophoblast spheroids with *HOXA10*KD cells. As evident in (movie S3) the epithelial cells juxtaposed to spheroid progressively moved away and at the end of 12h there was large zone of clearance around the spheroid (Fig 5 C).

To determine if loss of HOXA10 promoted epithelial cell displacement *in vivo*, we analyzed the implantation site of wild type and HOXA10 hypomorphs on D5 09:00h (Fig. 5 D). As expected, in the wild-type animals on D5 09:00h, cells in the implantation crypt were tightly held together and the LE was continuous (Fig. 5 D and E). In contrast, in the HOXA10 hypomorph on D5 09:00h itself, there were multiple gaps within the LE lining of the crypt suggestive of precocious epithelial cell displacement (Fig. 5 D and E). Thus, we conclude that the down-regulation of HOXA10 promotes pEMT in the LE for its displacement.

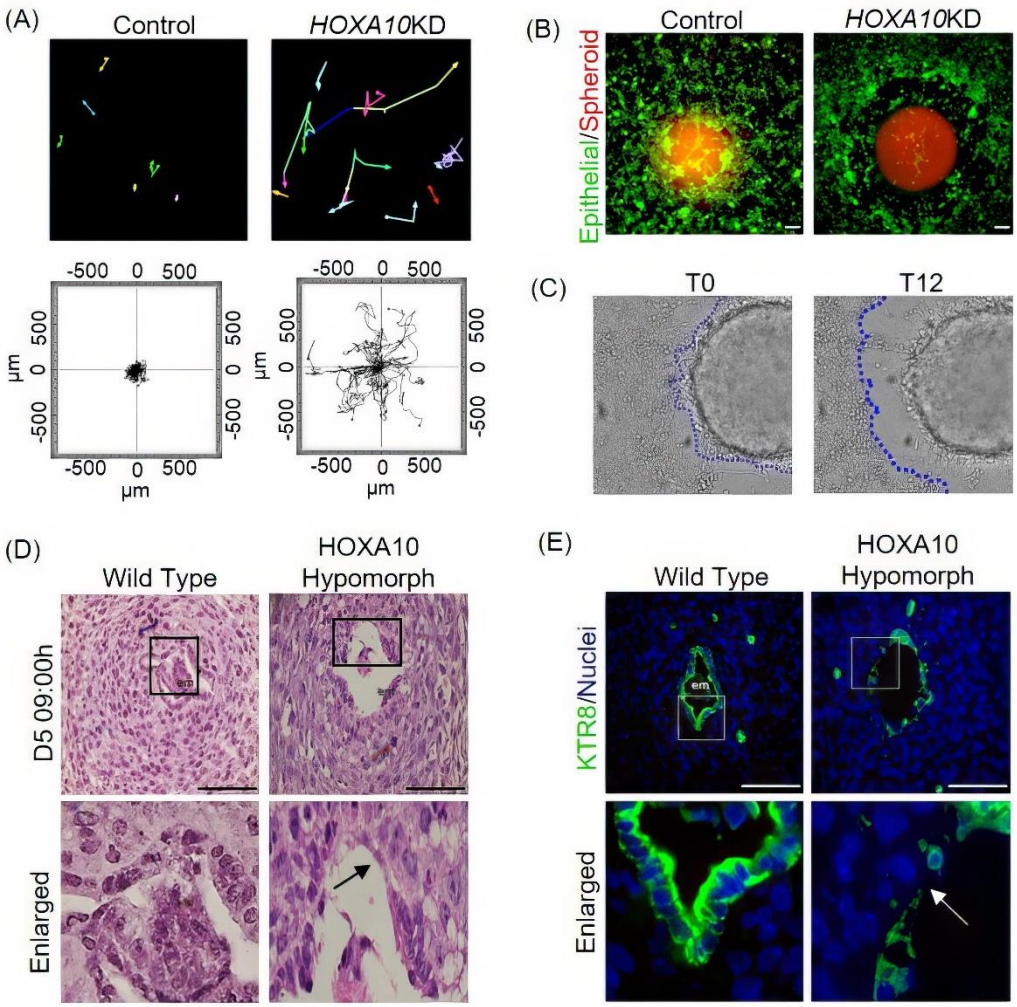

Fig. 5: Loss of HOXA10 drives migration of endometrial epithelial cells

Stable line of human endometrial epithelial cells (RL95-2) expressing scrambled shRNA (Control) and HOXA10 shRNA (*HOXA10*KD) were subjected to live imaging. (A) Tracks of control and *HOXA10*KD cells for 24h (Movie S1 and S2). Representative rose plots depicting the trajectories of control (n=22 cells) and *HOXA10*KD (n=22 cells) endometrial epithelial cells are also shown. (B) Displacement of endometrial epithelial cells in response to trophoblast spheroid. Monolayers of control and *HOXA10*KD cells were incubated with trophoblast spheroid and imaged after 24h. (C) Time-lapse of *HOXA10*KD cells incubated with trophoblast spheroid (Movie S3). Static images at T0 and T12 are shown. Marked are the boundaries of the epithelial cell layer. (D) Hematoxylin and Eosin-stained sections of wildtype and HOXA10 hypomorphs mouse uterus on D5 09:00h. (E) Immunofluorescence for KRT8 in wildtype and HOXA10 hypomorphs uteri on D5 09:00h. The selected area is boxed and zoomed. em = embryo. Scale bar = 100µm.

Loss of HOXA10 Promotes pEMT by Activating TGF-β Signaling Pathway

EMT involves one or more stable partial epithelial/mesenchymal (E/M) states that have a distinct gene signature profiles (46). Since the endometrial epithelial cells upon loss of HOXA10 display a pEMT phenotype, we performed RNAseq to determine their genetic signatures. Transcriptome analysis of *HOXA10*KD endometrial epithelial cells (RL95) revealed significant alterations in gene expression, with 2148 genes upregulated and 2915 genes downregulated as compared to control cells (Fig. 6 A). These differentially expressed genes (DEGs) were visualized in a heatmap, highlighting the substantial impact of HOXA10 knockdown on endometrial gene regulation. (SI Appendix, Fig. S6). We computed the pEMT scores and observed that *HOXA10*KD cells had a higher pEMT score as compared to controls (Fig. 6 B). We also computed the Pearson correlation coefficient of the differentially expressed genes with pEMT and HOXA10 and observed that genes that positively correlated with HOXA10 had negative correlation with pEMT scores and vice-versa (Fig. 6 C). Together this data demonstrated that *HOXA10*KD cells has a cellular transcriptome biased towards pEMT.

To determine the mechanisms by which HOXA10 drives pEMT, we performed GSEA of the DEGs. The gene ontology (GO) and pathways associated with these genes included tissue migration, actin filament-based movement, cell-substrate adhesion and cell junction assembly, all of which are known to occur in EMT (Fig. 6 D, SI Appendix, Fig. S7). To further investigate the impact of these DEGs on cellular function, GSEA of the genes involved in tissue migration was performed. The heatmap of the relevant DEGs reveled that almost equal proportion of genes were either upregulated or downregulated in *HOXA10*KD cells (SI Appendix, Fig. S8). The top 10 enriched biological processes were associated with TGF-β and PI3K-Akt signaling pathways. These genes were strongly interconnected with multiple processes associated with EMT including TGF-β signaling pathway (Fig. 6 E). To further dissect the association of HOXA10 and EMT, we curated a list of genes known to be involved in EMT from the EMTome and dbEMT datasets (55, 56). Of the 1918 genes that have known roles in EMT, 678 (35%) genes were differentially expressed in the *HOXA10*KD cells with several epithelial genes downregulated and mesenchymal genes being upregulated (Fig. 6 F)

GSEA of the 678 genes revealed their involvement in cell migration, cell-substrate adhesion, mesenchyme development, and response to TGF-β further corroborating the fact that loss of HOXA10 alters the EMT specific transcriptome including TGF-β (Fig. 6 G). We focused on the differentially abundant genes of the TGF-β signaling pathway (SI Appendix, Fig. S9) and observed that most of these genes had roles in mesenchyme development and tissue migration (Fig. 6 H). Interestingly, the inhibitors of TGF-β signaling were down-regulated while TGF-β

ligands, its receptors, and the SMADs were upregulated in *HOXA10*KD cells (Fig. 6 I). Treatment of TGF-β to human endometrial cell lines (including RL95) is known to induce EMT (57). Together this data implies that the loss of HOXA10 alters TGF-β signaling pathway gene network in the epithelial cell transcriptome to promote pEMT.

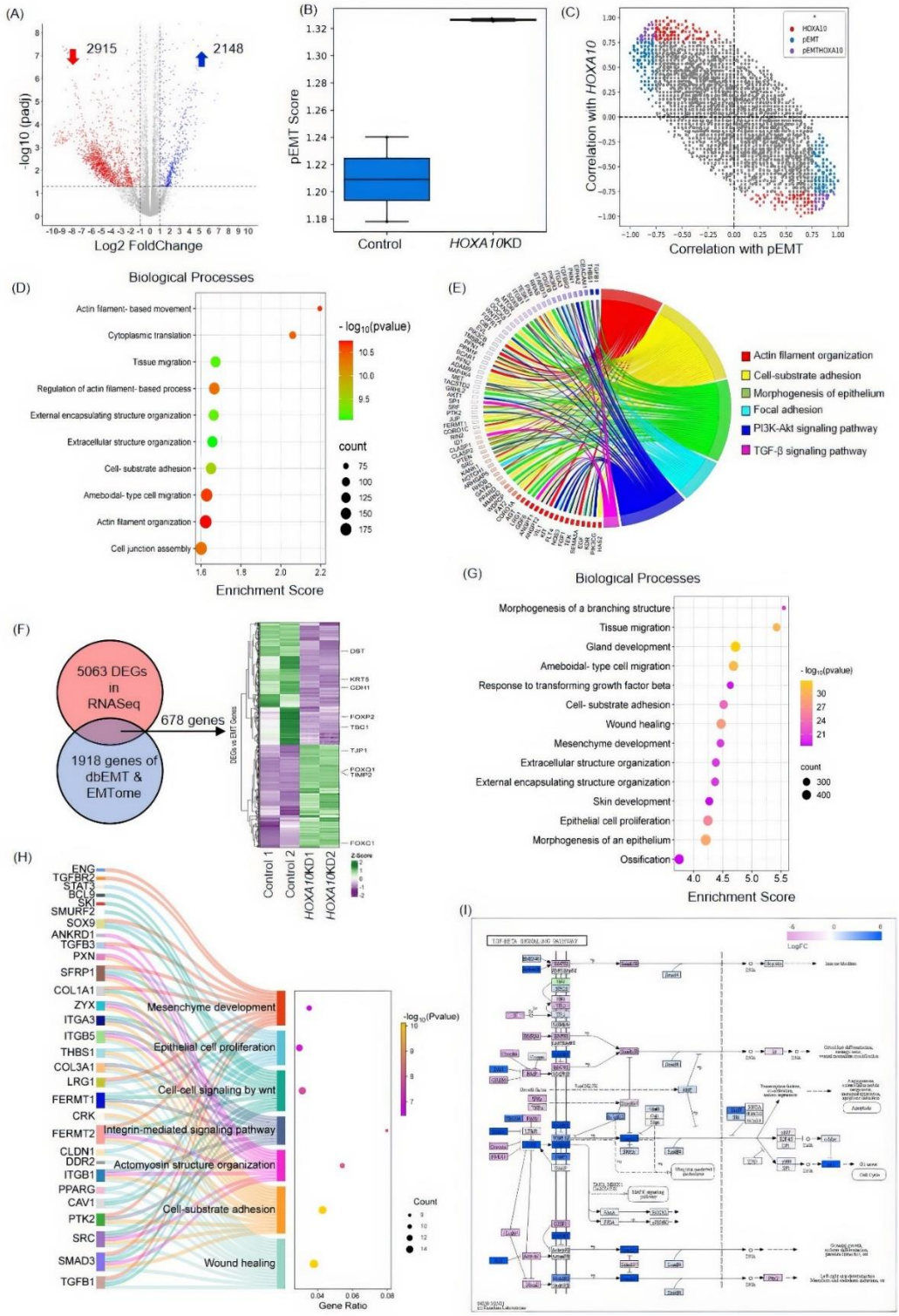

Fig. 6: Loss of HOXA10 alters endometrial epithelial cell transcriptome for partial EMT (pEMT)

(A) Volcano plot showing the differentially expressed genes between *HOXA10*KD and control. (B) pEMT scores (mean ±SD) computed from the transcriptomes of *HOXA10*KD and control cells. (C) Scatter plot of Pearson correlations between a gene and pEMT score versus its correlation with HOXA10 levels. Genes correlated with HOXA10, pEMT, or both are highlighted in red, blue, and purple, respectively. (D) Top enriched biological processes associated with the differentially expressed genes (DEGs). (E) GO-Chord plot depicting the third-tier GSEA of genes associated with tissue migration. (F) Venn diagram for the DEGs and genes in dbEMT & EMTome datasets to identify the EMT-associated genes. Heatmap of 678 differentially expressed EMT-associated genes. (G) The biological processes significantly enriched with 678 differentially expressed EMT-associated genes. (H) Sankey plot illustrates the flow of the differentially abundant genes involved in the TGF-β signaling pathway with the enriched biological processes. (I) KEGG pathway map of TGF-β signaling network highlighting the up and down-regulated genes in *HOXA10*KD cells.

HOXA10 Directly Suppresses Mesenchymal Genes and Activates the Epithelial Genes in the Endometrial Epithelial Cells

To investigate how HOXA10 regulates pEMT, we determined the HOXA10 binding sites in the human endometrial epithelial cell line (RL95). The chromatin occupancy of HOXA10 was measured by CUT&RUN using a validated antibody (SI Appendix, Fig. S3). We identified 69,990 high-confidence peaks in the HOXA10 CUT&RUN profile. We analyzed the top 10,000 peaks and observed that, (Fig.7 A) most were in the intergenic and intronic regions, a fraction of the peaks was enriched in the promoters and Transcription Start Site (TSS). MEME analysis of the top 5000 peaks revealed significant enrichment of motifs for large number of transcription factors including HOXA10. There was also significant enrichment of the binding motifs for CTCF (Fig. 7 B). Interestingly, enrichment of CTCF motif is reported in Chip Seq of HOXA10 in chicken cells (58), thereby validating our approach. Amongst the other motifs co-enriched with HOXA10 were those for FOXA2, KLF5, KLF9, KLF4 and FOXO1 (Fig. 7 B; SI Appendix, Table. S3). These genes have known roles in embryo implantation (S1 Appendix, Table. S4), as well as inducing mesenchymal to epithelial transition (MET) (59–61). We then sought to determine the functions of genes whose promoters and TSS were enriched in the HOXA10 cistrome. The result revealed that these genes were strongly associated with pathways related to cancers (including endometrial cancer), adherent junction, VEGF, HIPPO, and TGF-β signaling pathways (Fig. 7 C). Indeed gain/loss of HOXA10 is observed in many cancers (62, 63), and mice hypomorph for HOXA10 spontaneously develop

endometrial cancer (32). HOXA10 is also known to bind directly to the promoter of TGF-β and regulates its expression in human acute myeloid leukemia cells (64).

To identify the potential direct targets of HOXA10 in endometrial epithelial cells. We determined the proportion of genes whose promoters had HOXA10 occupancy and were dysregulated in the *HOXA10*KD cells. Of the 5378 high confidence peaks within the promoter/TSS, transcripts of 1246 (24.6%) genes were differentially expressed in *HOXA10*KD cells (Fig. 7 D). Analysis of 1246 direct target genes of HOXA10 revealed distinct gene expression patterns (Fig. 7 D). The upregulated HOXA10 direct targets were significantly enriched in biological process to EMT, actin remodeling, epithelial cell migration, and TGF-β signaling (Fig. 7 D). The related cellular component and pathways of the upregulated direct targets and GO terms associated with the downregulated direct targets is shown (SI Appendix, Fig. S10). We next assessed the occupancy of HOXA10 on key epithelial and mesenchymal genes. Towards this, we shortlisted six genes, three of which are expressed in the human endometrial epithelium (*CDH1, SDC1 and DST*, SI Appendix, Fig. S11), two genes of TGF-β signaling pathways (*TGFB1* and *SMAD3*) and *CDH2* (as a representation of mesenchymal phenotype). IGV tracks of these six genes revealed HOXA10 binding in the promoter region as well as throughout the gene body suggesting (Fig 7 E), that HOXA10 must directly regulate these genes. Indeed, of the six genes, the mRNA levels of all three epithelial genes were downregulated while those of the mesenchymal genes were upregulated in *HOXA10*KD cells as compared to control (Fig. 7 F). These results imply that HOXA10 maintains the epithelial phenotype by not just inducing the expression of epithelial genes but also suppressing the mesenchymal genes.

To address this further we analyzed the distribution of upregulated and downregulated direct HOXA10 target genes across six biological processes and associated KEGG signaling pathways involved in EMT. We observed that both groups of genes were evenly distributed across these categories, suggesting a broad impact of HOXA10 on EMT-related processes and pathways. (Fig. 7 G). Further analysis of the direct targets identified four distinct sets of PPI networks that fell into two broad categories viz those involved in epithelial function and those involved in mesenchymal functions (Fig. 7 H). Our analysis revealed several interconnected gene networks. Notably, we observed network of 10 genes implicated in epithelial development and another network of 14 genes involved in cell adhesion and cell junction formation, both crucial for epithelial phenotype. Furthermore, we also identified a network of 20 genes associated with TGF-β signaling and EMT. Importantly, this EMT-related network exhibited significant interactions with another network of genes involved in cell migration and motility

(Fig. 7 H). Together this data suggests that HOXA10 directly tunes the genes to maintain the epithelial phenotype, and its loss switches on the mesenchymal genes while maintaining or inducing a distinct set of epithelial genes resulting in a pEMT phenotype.

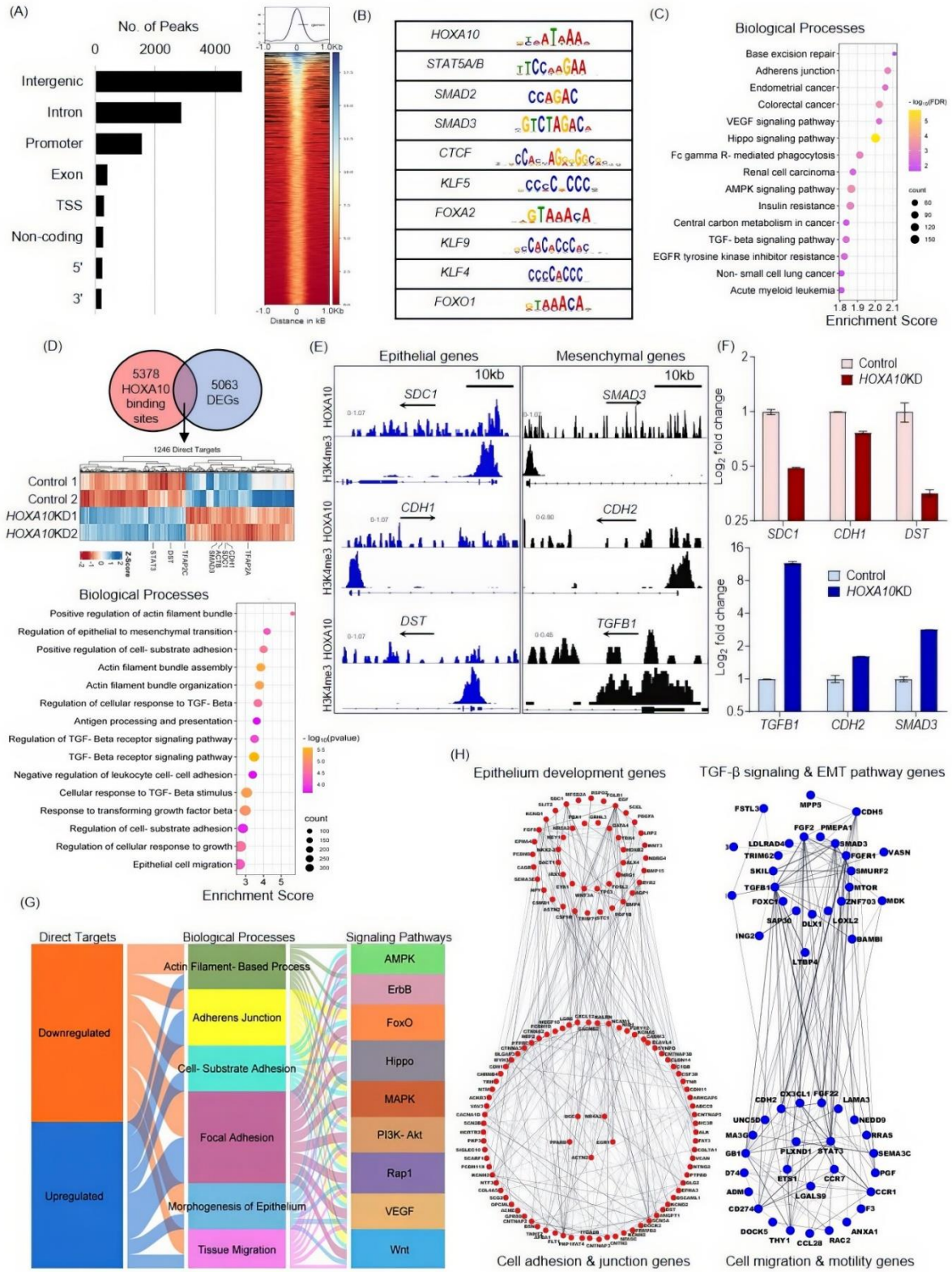

Fig. 7: HOXA10 directly suppresses mesenchymal genes and activates the epithelial gene for partial EMT (pEMT)

(A) Location statistics of top 10,000 high confidence peaks identified from CUR&RUN for HOXA10. The heat map and profile plot display the region occupied by HOXA10 in the endometrial epithelial cells. (B) Non-HOX motifs enriched in HOXA10 CUR&RUN. (C) Pathways associated with the genes that have HOXA10 occupancy on their promoters and transcription start site (TSS). (D) Direct targets of HOXA10 were identified as genes with promoters/TSS with HOXA10 occupancy and having differential expression in HOXA10 knockdown (*HOXA10*KD) RL95 cells. Heatmap depicts the expression of the direct target of HOXA10 in the control and *HOXA10*KD cells. (E) Occupancy of HOXA10 in three epithelial genes (*SDC1, DST, CDH1*) and three mesenchymal genes (*TGFB1, CDH2, SMAD3*) are shown in IGV plots, H3K4Me3 marks the promoters of the same genes. The arrow depicts the direction of gene transcription. (F) mRNA levels of three epithelial and three mesenchymal genes (shown in panel E) in the control vs *HOXA10*KD cells. Values are mean ±SD of the fold change compared to controls. (G) Distribution of direct target of HOXA10 across enriched biological processes and pathways associated with EMT. (H) Protein-protein interaction networks of the direct target of HOXA10 involved in epithelial and mesenchymal function.

Discussion

The results of the present study demonstrate that the endometrial luminal epithelial (LE) cells undergo pEMT which is essential for embryo implantation. The pEMT in the LE cells is driven by the loss of HOXA10 which activates the genes involved in the mesenchymal state while maintaining the expression of genes of epithelial state.

Histological observation of the implantation site of various species with invasive implantation has revealed that breaching the endometrial LE involves the intrusion of the trophectodermal projection between their intercellular junctions. The trophoblastic projections adhere to the lateral surfaces of the epithelial cells to loosen up the barrier and the embryo initiates breaching (65). However, before breaching, the LE cells at the site of implantation also lose their polarity, and become flattened, and there is an activation of some mesenchymal markers specifically at the site of implantation (28, 66–68). Extending these observations, herein we report that just after apposition and before embryo breaching, specifically in the LE of the implantation sites, there is a reduction in the expression of epithelial markers (E-Cad and KRT8) and activation of mesenchymal markers (N-Cad, ZEB2, TWIST2 and SNAIL) indicating the of occurrence of EMT. The LE cells at the site of embryo implantation, do not completely switch to the mesenchymal state but are in varying degrees of pEMT and the distribution of these states within the implantation crypt vary spatially. These observations provide conclusive evidence

that pEMT is activated in the endometrial LE at the embryo implantation site. The acquisition of the pEMT phenotype in the LE at this conjuncture is conceivable as it would aid in loosening up the tight epithelial cell-cell interactions to allow the trophoblastic protrusions to invade and adhere in between them. As pEMT cells have higher collective migratory properties (69), the switch in the LE cells would also help in the migration of the epithelial sheets that are required to accommodate the expanding blastocysts in the stromal/decidual bed (70).

EMT is induced by a core set of EMT-TFs mainly member of SNAI, ZEB and TWIST family. Referred to as the master regulators of EMT, gain of one or more members of these TF in epithelial cells induces EMT and its loss in mesenchymal cells drives MET (71–74). We profiled the expression of selected EMT-TFs at the implantation sites and observed that the LE cells on D5 morning expressed SNAIL, TWIST2 and ZEB2 while SLUG and ZEB1 were not detected suggesting that involvement of specific combination of core EMT-TFs during embryo implantation. Since TWIST2 was detected in the LE, early on at the time of embryo implantation, we knocked down its expression in the peri-implantation stage uterus. Loss of TWIST2 led to a significant reduction in the number of implantation sites and abnormally shaped implantation crypt in most animals. Interestingly, we also observed that on D6, in the control animals, the LE was completely cleared from the implantation sites; in the *Twist2* knockdown group, the LE cells were retained. These observations imply that the TWIST2 driven pEMT is essential for clearing the LE for embryo implantation. Interestingly, altered expression of epithelial cell polarity-related genes is reported in the endometrium of women with implantation failure and endometriosis (75–78). These observations imply that pEMT of the LE is essential for embryo implantation.

We next asked what are the genetic driver of pEMT at the time of implantation. HOXA10 is a transcription factor required for uterine biogenesis and essential for fertility (50). While HOXA10 is essential for the acquisition of endometrial receptivity, we and others have reported that its expression is downregulated specifically in the LE at the time of implantation in monkey and canine uterus (51, 52, 79). Herein, we also observed a significant reduction in the expression of HOXA10 in the LE of mouse and hamster uterus at the site of embryo implantation suggesting that it is an evolutionarily conserved phenomenon. This downregulation is not surprising as HOXA10 is progesterone receptor (PGR) responsive gene in the LE (80) and PGR expression is significantly downregulated in the LE on day 5 at the site of embryo implantation (81). Downregulation of HOXA10 in endometrial cells increases the expression of cytokines and growth factors like leukemia inhibiting factor (LIF), interleukin-15 (IL-15), IL-11, IL-6 and TGF-β (82), that are known to induce EMT (83–85). Also,

HOXA10 binds to the promoter of *CDH1* and increases its expression and also controls cytoskeletal remodeling in the endometrial epithelial cells (53, 86). These observations prompted us to hypothesize that HOXA10 may be required to maintain the epithelial phenotype in the endometrium and its loss may drive EMT in the endometrium. To test this, we knocked down HOXA10 in the human endometrial epithelial cells (RL95) and observed that these cells have a high pEMT score and co-expressed both the epithelial and mesenchymal markers. These *in vitro* observations were also corroborated *in vivo* where endometrial epithelial cells of mice hypomorphic for HOXA10 also co-expressed E-Cad and N-Cad indicating that loss of HOXA10 is sufficient to drive pEMT in the endometrial epithelium.

3D imaging of mouse endometrium has shown that the LE undergoes extensive folding (specifically on D5) to position the implantation crypt in close proximity to stroma (70). Such dynamic folding of the epithelium would require extensive migration of the epithelial sheets and EMT would certainly be required for such an activity. Indeed, altered LE folding and disrupted expression of EMT genes are observed in LE cells of mice knockout for planar cell polarity-related genes (87).To test if loss of HOXA10 drives cell migration we performed time -lapse imaging. While the control cells were minimally motile, these cells became highly migratory when *HOXA10* was knocked down. These observations demonstrate that loss of HOXA10 drives pEMT and the endometrial epithelial cells acquire a migratory phenotype. Static and live imaging of *in vitro* implantation assays have demonstrated that from the focal point of embryo adhesion, the endometrial cells are displaced and then migrate away (30, 88–90). To test if such directional migration is acquired by the epithelial cells upon loss of HOXA10, we co-incubated the *HOXA10*KD cells with trophoblast spheroids and observed that these cells moved away from the spheroid and created a space around it. Such descending motion of the epithelial cells would pave the way for the embryo to embed in to the endometrium. Due to experimental constraints, we cannot observe these phenomena directly *in vivo*, however, we did notice a precocious loss of the LE cells at the implantation site of the HOXA10 hypomorphs. These observations imply that loss of HOXA10 in the LE cells induces pEMT which makes the cells migratory and move away from the embryo providing an area for it to expand and invade into the stromal bed.

To understand the mechanistic basis of how the loss of HOXA10 drives pEMT, we performed RNAseq of control and *HOXA10*KD cells. Using previously validated methods (91), we calculated the pEMT scores and observed that compared to controls, the *HOXA10*KD human endometrial epithelial cells (RL95) had a higher pEMT score and there was a reciprocal relationship between genes that correlated with pEMT and HOXA10. Also, the biological

processes enriched for the genes differentially expressed upon loss of HOXA10 were associated with tissue migration, actin cytoskeletal organization, focal adhesions and TGF-β signaling pathways. All of these processes are known to be involved in EMT (92, 93), and their altered expression are observed in endometrium of women with implantation failure (18, 94). Interestingly, we observed that loss of HOXA10 in endometrial epithelial cells led to altered expression of nearly 35% of genes known to be involved in EMT and these genes were strongly associated with response to TGF-β. Interestingly, most upregulated genes were activators of TGF-β while their inhibitors were downregulated indicating that loss of HOXA10 may drive EMT in the endometrium by modulating the TGF-β pathway. Indeed, TGF-β is a key driver of EMT in most developmental conditions and also in cancers (95). Endometrial TGF-β is essential for implantation (96, 97), and the uterine epithelium of mice knockout for the TGF-β receptor ALK3 has higher expression of the E-Cad, and cell junctions proteins indicative of failure of EMT (98). These observations prompt us to speculate that the loss of HOXA10 in the endometrial epithelium may activate TGF-β to drive EMT for embryo implantation.

We next sought to determine the genome-wide binding preference of HOXA10 in endometrial epithelial cells. We observed that in HOXA10 cistrome there is an enrichment of motifs for transcription factors which are essential for embryo implantation (SI Appendix, Table 4). In addition, we observed motif for STAT and KLF family of TF. Interestingly, KLFs are known to be involved in MET (59–61); STAT3 is elevated in the LE at the time of embryo implantation (99) and increased expression of epithelium junction complex protein like claudin are observed in mice knockout for *Stat3* in the LE (100). These findings prompt us to propose that embryo implantation requires interaction of the core set of transcription factors which would cooperatively control the epithelium transcriptome for EMT/MET states for embryo attachment and invasion.

Mathematical modeling and experimental data have suggested that multiple partial and stable E/M states can be acquired due to collective interactions amongst the genes involved in the EMT gene regulatory networks and perturbations in the network topology is the determinant of the emergence of the pEMT phenotypes (101, 102). To determine if HOXA10 is a part of such an EMT gene regulatory network, we first defined a core set of genes that are direct targets of HOXA10 in endometrial epithelial cells. The 1246 direct targets were enriched for GO terms such as EMT, tissue migration, and epithelial morphogenesis; significant HOXA10 occupancy was observed on promoters of mesenchymal and epithelial genes that were differentially expressed upon *HOXA10* knockdown. These observations indicate that HOXA10 must be a member of the EMT gene regulatory network in endometrial cells. Indeed, amongst the direct

targets, four distinct sets of PPI networks were identified that fell into two broad categories viz those involved in epithelial function and those involved in mesenchymal functions and these networks exhibited significant interactions with another network of genes involved in cell migration and motility. We also observed that the upregulated and downregulated direct targets were evenly distributed across all the biological processes and KEGG pathways involved in EMT. These observations indicate that the acquisition of a partial state in the EMT spectrum involves a well-calibrated regulation of sub-networks where specific genes in one network need to be suppressed while upregulating members of the opposite network. Indeed mathematical modeling has predicted the existence of multiple mutually inhibitory networks as a characteristic feature of pEMT (27, 61, 103). Our results suggest that in the endometrial epithelium, higher HOXA10 expression would keep the cells towards an epithelial network state while suppressing the mesenchymal networks. Therefore, HOXA10 can be consider as a member of the 'team' of MET inducers that engage in mutually inhibitory feedback loops directly or indirectly with EMT inducers.

In summary, the present study has identified endometrial EMT as a key step in the process of embryo implantation. In light of our work, it is evident that in the receptive endometrium, once the embryo has apposed, the loss of HOXA10 in LE drives the cells toward pEMT state. The maintenance of the epithelial state would aid in embryonic trophoblast attachment. While the acquisition of the mesenchymal state would aid in movements of the epithelial layer paving a way for the embryo to embed in the stroma. This discovery is a significant leap in expanding our understanding of the basic mechanisms of embryo implantation, a bottleneck in success of IVF. These findings would assist in designing effective modalities to improve implantation rates in couples undergoing assisted reproduction. In addition, the discovery that HOXA10 is essential to control epithelial identity in the endometrium would also have broader implications in understanding many endometrial disorders including cancers as both aberrant HOXA10 expression and EMT are involved in the pathogenesis of these conditions.

Data Availability

All data generated in this study is available at European Nucleotide Archive (ENA) with Accession Number PRJEB82872 (RNA-seq data) and PRJEB83114 (CUT&RUN data).

Acknowledgement: We are grateful to Varun Suresh and Saee Patil for valuable technical inputs, we are thankful to Dr Geetanjali Sachdeva (ICMR-NIRRCH) for kind gift of RL95-2 cells, we are thankful to Dr Bhakti Pathak (ICMR-NIRRCH) for inputs in establishing stable

clones. This work was supported by grants from Department of Science and Technology - Science and Engineering Research Board (DST No: CRG/2018/002314) and Department of Biotechnology (BT/PR51181/MED/97/675/2023). DM lab is funded by grants from the Indian Council of Medical Research (ICMR), Govt. of India. NA and AM are recipient of ICMR-Senior Research Fellowship. S Shyamal is thankful to Department of Biotechnology-BioCARe for funding (BT/PR50903/BIC/101/1307/2023), SH is thankful for Institution of Eminence, Banaras Hindu University (IoE- BHU), PDF (6031) for funding, HBV is thankful for Prime Minister's Research Fellowship (PMRF), MKJ supported by Param Hansa philanthropies. The manuscript bears the NIRRCH ID: RA/1817/01-2025.

References

1. D. J. Stadtmauer, G. P. Wagner, The Primacy of Maternal Innovations to the Evolution of Embryo Implantation. *Integr. Comp. Biol.* **60**, 742 (2020).
2. N. Ashary, A. Tiwari, D. Modi, Embryo Implantation: War in Times of Love. *Endocrinology* **159**, 1188–1198 (2018).
3. Y. Fukui, *et al.*, Uterine receptivity, embryo attachment, and embryo invasion: Multistep processes in embryo implantation. *Reprod. Med. Biol.* **18**, 234–240 (2019).
4. M. A. Ochoa-Bernal, A. T. Fazleabas, Physiologic Events of Embryo Implantation and Decidualization in Human and Non-Human Primates. *Int. J. Mol. Sci.* **21** (2020).
5. M. G. Elliot, B. J. Crespi, Phylogenetic Evidence for Early Hemochorial Placentation in Eutheria. *Placenta* **30**, 949–967 (2009).
6. D. Siriwardena, T. E. Boroviak, Evolutionary divergence of embryo implantation in primates. *Philos. Trans. R. Soc. B* **377** (2022).
7. A. M. El Shershaby, J. R. Hinchliffe, Epithelial autolysis during implantation of the mouse blastocyst: an ultrastructural study. *Development* **33**, 1067–1080 (1975).
8. A. O. Welsh, A. C. Enders, Chorioallantoic placenta formation in the rat. III. Granulated cells invade the uterine luminal epithelium at the time of epithelial cell death. *Biol. Reprod.* **49**, 38–57 (1993).
9. E. L. Parr, H. N. Tung, M. B. Parr, Apoptosis as the mode of uterine epithelial cell death during embryo implantation in mice and rats. *Biol. Reprod.* **36**, 211–225 (1987).
10. Y. Li, X. Sun, S. K. Dey, Entosis Allows Timely Elimination of the Luminal Epithelial Barrier for Embryo Implantation. *Cell Rep.* **11**, 358 (2015).
11. S. Akaeda, *et al.*, Retinoblastoma protein promotes uterine epithelial cell cycle arrest and necroptosis for embryo invasion. *EMBO Rep.* **22** (2021).

12. R.-W. Su, *et al.*, Junctional Adhesion Molecule 2 Mediates the Interaction between Hatched Blastocyst and Luminal Epithelium: Induction by Progesterone and LIF. *PLoS One* **7**, e34325 (2012).
13. X. Ye, Uterine Luminal Epithelium as the Transient Gateway for Embryo Implantation. *Trends Endocrinol. Metab.* **31**, 165–180 (2020).
14. C. R. Murphy, Junctional barrier complexes undergo major alterations during the plasma membrane transformation of uterine epithelial cells. *Hum. Reprod.* **15**, 182–188 (2000).
15. A. Hochfeld, H. M. Beier, H.-W. Denker, Changes of Intermediate Filament Protein Localization in Endometrial Cells During Early Pregnancy of Rabbits. *Trophobl. Invasion Endometrial Recept.* 357–374 (1990). https://doi.org/10.1007/978-1-4613-0615-3_19.
16. M. Thie1, *et al.*, Cell adhesion to the apical pole of epithelium: a function of ce11 polarity. *Eur. J. Cell Biol.* **66**, 180–191 (1995).
17. R. K. Jha, S. Titus, D. Saxena, P. G. Kumar, M. Laloraya, Profiling of E-cadherin, beta-catenin and Ca(2+) in embryo-uterine interactions at implantation. *FEBS Lett.* **580**, 5653–5660 (2006).
18. N. Deng, *et al.*, H3K27me3 timely dictates uterine epithelial transcriptome remodeling and thus transformation essential for normal embryo implantation. *Cell Death Differ. 2024 318* **31**, 1013–1028 (2024).
19. J. S. Dudley, C. R. Murphy, M. B. Thompson, B. M. McAllan, Uterine cellular changes during mammalian pregnancy and the evolution of placentation. *Biol. Reprod.* **105**, 1381–1400 (2021).
20. J. Yuan, *et al.*, Planar cell polarity signaling in the uterus directs appropriate positioning of the Crypt for Embryo implantation. *Proc. Natl. Acad. Sci. U. S. A.* **113**, E8079–E8088 (2016).
21. Y. S. Kim, *et al.*, An unanticipated discourse of HB-EGF with VANGL2 signaling during embryo implantation. *Proc. Natl. Acad. Sci. U. S. A.* **120**, e2302937120 (2023).
22. H. Y. Jung, *et al.*, Apical–basal polarity inhibits epithelial–mesenchymal transition and tumour metastasis by PAR-complex-mediated SNAI1 degradation. *Nat. Cell Biol. 2019 213* **21**, 359–371 (2019).
23. F. Peglion, S. Etienne-Manneville, Cell polarity changes in cancer initiation and progression. *J. Cell Biol.* **223** (2024).
24. R. Kalluri, R. A. Weinberg, The basics of epithelial-mesenchymal transition. *J. Clin.*

Invest. **119**, 1420 (2009).

25. C. Kröger, *et al.*, Acquisition of a hybrid E/M state is essential for tumorigenicity of basal breast cancer cells. *Proc. Natl. Acad. Sci. U. S. A.* **116**, 7353–7362 (2019).
26. R. J. Norgard, *et al.*, Calcium signaling induces a partial EMT. *EMBO Rep.* **22** (2021).
27. A. R. Subbalakshmi, S. Sahoo, K. Biswas, M. K. Jolly, A Computational Systems Biology Approach Identifies SLUG as a Mediator of Partial Epithelial-Mesenchymal Transition (EMT). *Cells. Tissues. Organs* **211**, 689–702 (2022).
28. A. Tiwari, N. Ashary, N. Singh, S. Sharma, D. Modi, Modulation of E-Cadherin and N-Cadherin by ovarian steroids and embryonic stimuli. *Tissue Cell* **73** (2021).
29. H. Uchida, *et al.*, How to Create an Embryo Penetration Route. *Am. J. Reprod. Immunol.* **75**, 326–332 (2016).
30. H. Uchida, *et al.*, Studies using an in vitro model show evidence of involvement of epithelial-mesenchymal transition of human endometrial epithelial cells in human embryo implantation. *J. Biol. Chem.* **287**, 4441–4450 (2012).
31. H. W. Denker, Implantation: Cell biology of embryo penetration route revisited. *Am. J. Reprod. Immunol.* **76**, 429–431 (2016).
32. A. Mishra, N. Ganguli, S. S. Majumdar, D. Modi, Loss of HOXA10 causes endometrial hyperplasia progressing to endometrial cancer. *J. Mol. Endocrinol.* **69**, 431–444 (2022).
33. J. Reese, H. Wang, T. Ding, B. C. Paria, The hamster as a model for embryo implantation: Insights into a multifaceted process. *Semin. Cell Dev. Biol.* **19**, 194–203 (2008).
34. A. Mishra, M. Galvankar, S. Vaidya, U. Chaudhari, D. Modi, Mouse model for endometriosis is characterized by proliferation and inflammation but not epithelial-to-mesenchymal transition and fibrosis. *J. Biosci.* **45**, 1–15 (2020).
35. N. Singh, *et al.*, LHX2 in germ cells control tubular organization in the developing mouse testis. *Exp. Cell Res.* **425** (2023).
36. N. J. Hannan, P. Paiva, E. Dimitriadis, L. A. Salamonsen, Models for Study of Human Embryo Implantation: Choice of Cell Lines? *Biol. Reprod.* **82**, 235–245 (2010).
37. Z. Ban, F. Knöspel, M. R. Schneider, Shedding light into the black box: Advances in in vitro systems for studying implantation. *Dev. Biol.* **463**, 1–10 (2020).
38. M. Thie, *et al.*, Adhesiveness of the free surface of a human endometrial monolayer for trophoblast as related to actin cytoskeleton. *Mol. Hum. Reprod.* **3**, 275–283 (1997).
39. M. P. Iwanicki, *et al.*, Ovarian cancer spheroids use myosin-generated force to clear

the mesothelium. *Cancer Discov.* **1**, 144–157 (2011).

40. P. J. Skene, S. Henikoff, An efficient targeted nuclease strategy for high-resolution mapping of DNA binding sites. *Elife* **6** (2017).
41. F. N. de Mello, A. C. Tahira, M. G. Berzoti-Coelho, S. Verjovski-Almeida, The CUT&RUN greenlist: genomic regions of consistent noise are effective normalizing factors for quantitative epigenome mapping. *Brief. Bioinform.* **25** (2024).
42. J. M. Elizarraras, *et al.*, WebGestalt 2024: faster gene set analysis and new support for metabolomics and multi-omics. *Nucleic Acids Res.* **52**, W415–W421 (2024).
43. C. Xie, *et al.*, KOBAS 2.0: a web server for annotation and identification of enriched pathways and diseases. *Nucleic Acids Res.* **39** (2011).
44. D. A. Barbie, *et al.*, Systematic RNA interference reveals that oncogenic KRAS-driven cancers require TBK1. *Nature* **462**, 108–112 (2009).
45. Z. Fang, X. Liu, G. Peltz, GSEApy: a comprehensive package for performing gene set enrichment analysis in Python. *Bioinformatics* **39** (2023).
46. S. V. Puram, *et al.*, Single-Cell Transcriptomic Analysis of Primary and Metastatic Tumor Ecosystems in Head and Neck Cancer. *Cell* **171**, 1611-1624.e24 (2017).
47. P. Virtanen, *et al.*, SciPy 1.0: fundamental algorithms for scientific computing in Python. *Nat. Methods* **17**, 261–272 (2020).
48. D. Sinha, P. Saha, A. Samanta, A. Bishayee, Emerging Concepts of Hybrid Epithelial-to-Mesenchymal Transition in Cancer Progression. *Biomol. 2020, Vol. 10, Page 1561* **10**, 1561 (2020).
49. N. Ashary, S. Laheri, D. Modi, Homeobox genes in endometrium: from development to decidualization. *Int J Dev Biol* **64**, 227–37 (2020).
50. A. Mishra, D. Modi, Role of HOXA10 in pathologies of the endometrium. *Rev. Endocr. Metab. Disord. 2024* 1–16 (2024). https://doi.org/10.1007/S11154-024-09923-8.
51. D. Modi, G. Godbole, HOXA10 signals on the highway through pregnancy. *J. Reprod. Immunol.* **83**, 72–78 (2009).
52. G. B. Godbole, D. N. Modi, C. P. Puri, Regulation of homeobox A10 expression in the primate endometrium by progesterone and embryonic stimuli. *Reproduction* **134**, 513–523 (2007).
53. Y. Bi, *et al.*, HOXA10 improves endometrial receptivity by upregulating E-cadherin†. *Biol. Reprod.* **106**, 992–999 (2022).
54. H. Yoshida, R. Broaddus, W. Cheng, S. Xie, H. Naora, Deregulation of the HOXA10

homeobox gene in endometrial carcinoma: role in epithelial-mesenchymal transition. *Cancer Res.* **66**, 889–897 (2006).

55. M. Zhao, Y. Liu, C. Zheng, H. Qu, dbEMT 2.0: An updated database for epithelial-mesenchymal transition genes with experimentally verified information and precalculated regulation information for cancer metastasis. *J. Genet. Genomics* **46**, 595–597 (2019).
56. S. V. Vasaikar, *et al.*, EMTome: a resource for pan-cancer analysis of epithelial-mesenchymal transition genes and signatures. *Br. J. Cancer 2020 1241* **124**, 259–269 (2020).
57. L. Muinelo-Romay, *et al.*, High-risk endometrial carcinoma profiling identifies TGF-β1 as a key factor in the initiation of tumor invasion. *Mol. Cancer Ther.* **10**, 1357–1366 (2011).
58. I. Jerković, *et al.*, Genome-Wide Binding of Posterior HOXA/D Transcription Factors Reveals Subgrouping and Association with CTCF. *PLOS Genet.* **13**, e1006567 (2017).
59. T. Wang, *et al.*, A negative feedback loop between KLF9 and the EMT program dictates metastasis of hepatocellular carcinoma. *J. Cell. Mol. Med.* **27**, 2372 (2023).
60. D. Bhargava, D. Rusakow, W. Zheng, S. Awad, J. P. Katz, KLF5 inhibition initiates epithelial-mesenchymal transition in non-transformed human squamous epithelial cells. *Biochim. Biophys. acta. Mol. cell Res.* **1871** (2024).
61. A. R. Subbalakshmi, *et al.*, Klf4 induces mesenchymal–epithelial transition (Met) by suppressing multiple emt-inducing transcription factors. *Cancers (Basel).* **13**, 5135 (2021).
62. D. Gong, *et al.*, Overexpression of HOXA10 promotes the growth and metastasis of nasopharyngeal carcinoma. *Exp. Biol. Med. (Maywood).* **246**, 2454–2462 (2021).
63. R. Chen, *et al.*, Loss of nuclear functions of HOXA10 is associated with testicular cancer proliferation. *Front. Oncol.* **8** (2018).
64. C. A. Shah, H. Wang, L. Bei, L. C. Platanias, E. A. Eklund, HoxA10 Regulates Transcription of the Gene Encoding Transforming Growth Factor β2 (TGFβ2) in Myeloid Cells. *J. Biol. Chem.* **286**, 3161–3176 (2011).
65. H. Wang, S. K. Dey, Roadmap to embryo implantation: clues from mouse models. *Nat. Rev. Genet.* **7**, 185–199 (2006).
66. X. Cheng, *et al.*, NLRP3 promotes endometrial receptivity by inducing epithelial-mesenchymal transition of the endometrial epithelium. *Mol. Hum. Reprod.* **27**, 1–13 (2021).

67. J. Gou, *et al.*, Role of epithelial-mesenchymal transition regulated by twist basic helix-loop-helix transcription factor 2 (Twist2) in embryo implantation in mice. *Reprod. Fertil. Dev.* **31**, 932–940 (2019).
68. Z. Xu, *et al.*, ZEB1 Promotes Epithelial-Mesenchymal Transition of Endometrial Epithelial Cells and Plays a Critical Role in Embryo Implantation in Mice. *Reprod. Sci.* (2024). https://doi.org/10.1007/S43032-024-01646-0.
69. K. Saxena, M. K. Jolly, K. Balamurugan, Hypoxia, partial EMT and collective migration: Emerging culprits in metastasis. *Transl. Oncol.* **13**, 100845 (2020).
70. M. K. Madhavan, *et al.*, Aberrant uterine folding in mice disrupts implantation chamber formation and alignment of embryo-uterine axes. *Development* **149** (2022).
71. M. Saitoh, Transcriptional regulation of EMT transcription factors in cancer. *Semin. Cancer Biol.* **97**, 21–29 (2023).
72. P. Debnath, R. S. Huirem, P. Dutta, S. Palchaudhuri, Epithelial-mesenchymal transition and its transcription factors. *Biosci. Rep.* **42** (2022).
73. T. Kim, *et al.*, p53 regulates epithelial–mesenchymal transition through microRNAs targeting ZEB1 and ZEB2. *J. Exp. Med.* **208**, 875–883 (2011).
74. P. Dong, *et al.*, MiR-137 and miR-34a directly target Snail and inhibit EMT, invasion and sphere-forming ability of ovarian cancer cells. *J. Exp. Clin. Cancer Res.* **35**, 1–9 (2016).
75. S. Whitby, W. Zhou, E. Dimitriadis, Alterations in Epithelial Cell Polarity During Endometrial Receptivity: A Systematic Review. *Front. Endocrinol. (Lausanne).* **11** (2020).
76. L. Konrad, *et al.*, Epithelial–Mesenchymal Transition in Endometriosis—When Does It Happen? *J. Clin. Med. 2020, Vol. 9, Page 1915* **9**, 1915 (2020).
77. U. K. Soni, *et al.*, A high level of TGF-B1 promotes endometriosis development via cell migration, adhesiveness, colonization, and invasiveness. *Biol. Reprod.* **100**, 917–938 (2019).
78. R. Kakar-Bhanot, *et al.*, Rab11a drives adhesion molecules to the surface of endometrial epithelial cells. *Hum. Reprod.* **34**, 519–529 (2019).
79. B. Guo, *et al.*, Expression and hormonal regulation of Hoxa10 in canine uterus during the peri-implantation period. *Reprod. Domest. Anim.* **44**, 638–642 (2009).
80. M. Gebril, *et al.*, Uterine Epithelial Progesterone Receptor Governs Uterine Receptivity Through Epithelial Cell Differentiation. *Endocrinology* **161** (2020).
81. J. Tan, B. C. Paria, S. K. Dey, S. K. Das, Differential uterine expression of estrogen

and progesterone receptors correlates with uterine preparation for implantation and decidualization in the mouse. *Endocrinology* **140**, 5310–5321 (1999).

82. G. Godbole, *et al.*, Decrease in Expression of HOXA10 in the Decidua After Embryo Implantation Promotes Trophoblast Invasion. *Endocrinology* **158**, 2618–2633 (2017).
83. X. Yue, *et al.*, Leukemia inhibitory factor promotes EMT through STAT3-dependent miR-21 induction. *Oncotarget* **7**, 3777–3790 (2016).
84. K. S. Ásgeirsson, K. Ólafsdóttir, J. G. Jónasson, H. M. Ógmundsdóttir, The effects of IL-6 on cell adhesion and e-cadherin expression in breast cancer. *Cytokine* **10**, 720–728 (1998).
85. I. Ray, A. Michael, L. B. Meira, P. E. Ellis, The Role of Cytokines in Epithelial–Mesenchymal Transition in Gynaecological Cancers: A Systematic Review. *Cells* **12** (2023).
86. A. N. Kallen, K. Haines, H. S. Taylor, HOXA10 Regulates Expression of Cytokeratin 15 in Endometrial Epithelial Cytoskeletal Remodeling. *Reprod. Sci.* **21**, 892–897 (2014).
87. E. R. Roberts, *et al.*, Loss of PRICKLE1 leads to abnormal endometrial epithelial architecture, decreased embryo implantation, and reduced fertility in mice. *bioRxiv Prepr. Serv. Biol.* (2024). https://doi.org/10.1101/2024.08.06.605120.
88. P. T. Ruane, *et al.*, Trophectoderm differentiation to invasive syncytiotrophoblast is promoted by endometrial epithelial cells during human embryo implantation. *Hum. Reprod.* **37**, 777 (2022).
89. H. Wang, *et al.*, A novel model of human implantation: 3D endometrium-like culture system to study attachment of human trophoblast (Jar) cell spheroids. *Mol. Hum. Reprod.* **18**, 33–43 (2012).
90. S. Shibata, *et al.*, Modeling embryo-endometrial interface recapitulating human embryo implantation. *Sci. Adv.* **10** (2024).
91. S. V. Puram, *et al.*, Single-Cell Transcriptomic Analysis of Primary and Metastatic Tumor Ecosystems in Head and Neck Cancer. *Cell* **171**, 1611-1624.e24 (2017).
92. A. Datta, *et al.*, Cytoskeletal Dynamics in Epithelial-Mesenchymal Transition: Insights into Therapeutic Targets for Cancer Metastasis. *Cancers 2021, Vol. 13, Page 1882* **13**, 1882 (2021).
93. S. Brabletz, H. Schuhwerk, T. Brabletz, M. P. Stemmler, Dynamic EMT: a multi-tool for tumor progression. *EMBO J.* **40** (2021).
94. V. Chettiar, A. Patel, S. S. Chettiar, D. D. Jhala, Meta-analysis of endometrial

transcriptome data reveals novel molecular targets for recurrent implantation failure. *J. Assist. Reprod. Genet.* **41**, 1417–1431 (2024).

95. J. H. Lee, J. Massagué, TGF-β in developmental and fibrogenic EMTs. *Semin. Cancer Biol.* **86**, 136–145 (2022).
96. V. K. Maurya, *et al.*, Transforming growth factor-beta 1 (TGF-B1) liberation from its latent complex during embryo implantation and its regulation by estradiol in mouse. *Biol. Reprod.* **89** (2013).
97. R. L. Jones, C. Stoikos, J. K. Findlay, L. A. Salamonsen, TGF-β superfamily expression and actions in the endometrium and placenta. *Reproduction* **132**, 217–232 (2006).
98. D. Monsivais, *et al.*, Uterine ALK3 is essential during the window of implantation. *Proc. Natl. Acad. Sci. U. S. A.* **113**, E387–E395 (2016).
99. T. Hiraoka, *et al.*, Differential roles of uterine epithelial and stromal STAT3 coordinate uterine receptivity and embryo attachment. *Sci. Rep.* **10** (2020).
100. S. Pawar, *et al.*, STAT3 regulates uterine epithelial remodeling and epithelial-stromal crosstalk during implantation. *Mol. Endocrinol.* **27**, 1996–2012 (2013).
101. M. Rashid, K. Hari, J. Thampi, N. K. Santhosh, M. K. Jolly, Network topology metrics explaining enrichment of hybrid epithelial/mesenchymal phenotypes in metastasis. *PLOS Comput. Biol.* **18**, e1010687 (2022).
102. P. Jain, *et al.*, Cell-state transitions and density-dependent interactions together explain the dynamics of spontaneous epithelial-mesenchymal heterogeneity. *iScience* **27**, 110310 (2024).
103. M. K. Jolly, *et al.*, Implications of the Hybrid Epithelial/Mesenchymal Phenotype in Metastasis. *Front. Oncol.* **5** (2015).